Chapter 7

Measurement of polarization leakage

Mechanical and electronic imperfections can result into polarization leakage in individual antennas of a radio interferometer. Such leakages manifest themselves as closure errors even in *co-polar* visibility measurements of unpolarized sources. Towards the very end of this dissertation, work was done to develope and test a method for the computation of polarization leakage for radio interferometric telescopes using *only* the nominally *co-polar* visibilities. This chapter describes the work done in this direction (Bhatnagar & Nityananda , in press).

7.1 Introduction

The mutual coherence function (also called the visibility function) for an unresolved and unpolarized source, measured by an interferometer array can be modeled as a product of antenna based complex gains. These complex gains can be derived from the measured visibility function using the standard algorithm, which we call `antsol`. `antsol` forms the central engine of most amplitude and phase calibration schemes used for radio interferometric data. (The earliest published reference for an algorithm for `antsol` of which we are aware is Thompson & D'Addario (1982)).

Usually antenna feeds measure the components of the incident radiation along two orthogonal polarization states by two separate feeds. The signals from the two feeds travel through essentially independent paths till the correlator. However, due to mechanical imperfections in the feed or imperfections in the electronics, the two signals can leak into each other at various points in the signal chain.

At the correlator, signals from all the antennas are multiplied with each other and the results averaged to produce the visibilities. The signals of same polarization are multiplied to produce the *co-polar* visibilities while the signals of orthogonal polarizations are multiplied to produce the *cross-polar* visibilities. The *co-polar* and *cross-polar* visibilities can be used to compute the full Stokes visibility function. Antenna based instrumental polarization and polarization leakage can be derived from the full Stokes coherence function for a source of known structure (usually an unresolved source) (Hamaker et al. 1996; Sault et al. 1996, henceforth HBS).

The correlator used for the Giant Metrewave Radio Telescope (GMRT) by default computes the *co-polar* visibilities using the *Indian mode* of the VLBA Multiplier and Accumulator (MAC) chip. Here we describe a method, which we call `leaky antsol`, for the computation of the leakages using *only* the *co-polar* visibility function for an unpolarized source. Following the notation used by HBS, we label the two orthogonal polarizations by p and q to remind us that the formulation is independent of the precise orthogonal pair of polarization states chosen.

Section 7.2 describes the motivation which led to this analysis. For orientation, Section 7.3 starts with the problem of solving for the usual complex antenna based gains and sets up an iterative scheme for the solution. The problem of *simultaneously* solving for the complex antenna gains and leakages is then posed in Section 7.3.1 and a similar iterative scheme is set up. Section 7.3.2 presents the results of the simulations done to test the scheme. Section 7.4.1 presents some results using the GMRT at 150 MHz. Also, we were fortunate to have the L-band feeds of one of the GMRT antennas converted from linear to circular polarization. We observed `3C147` in this mode where all baselines with this special antenna measured the correlation between nominally linear and circular polarization. Results of this experiment demonstrate that the leakage solutions are indeed giving information about the polarization properties of the feeds. These results and their interpretation on the Poincaré sphere are presented in section 7.4.2. Section 7.5 gives the interpretation of the leakage solutions and discusses closure errors due to polarization leakage using the Poincaré sphere.

7.2 Motivation

Rogers (1983) pointed out in the context of the VLBA, that the polarization leakage cause closure errors even in nominally *co-polar* visibilities. Massi et al. (1997) have carried out a detailed study of this effect for the telescopes of the European VLBI Network (EVN). The motivation behind this word was that the current single sideband GMRT correlator uses the so called *Indian mode* of the VLBA MAC chips to produce only the *co-polar* visibilities. Also, the planned Walsh switching has not yet been implemented at the GMRT and in any case, would not eliminate leakage generated before the switching point. Tests done using strong point source dominated fields show unaccounted closure errors at a few percent level. The motivation behind developing an algorithm to solve for gains and leakages simultaneously, using *only* the *co-polar* visibilities was to determine if the measured closure errors could be due to polarization leakage in the system. Estimates of leakage can then be used in the primary calibration to remove the effects of polarization leakage. This is where this work differs from the earlier work of HBS which is about the calibration using the full Stokes visibility function, needed for observations of polarized sources. The polarization leakage in some of the EVN antennas corrupts the *co-polar* visibilities at a level visible as a reduction in the dynamic range of the maps (Massi & Aaron 1997a,b; Massi et al. 1998). Thus such a method can also be used in imaging data from the EVN and other telescopes affected by such closure errors.

Let g_i^p represent the complex gain for the p-polarization channel of the i^{th} antenna and α_i^q represent the leakage[1] of the *q*-polarization signal into the *p*-polarization channel. The electric field measured by antenna i can then be written as

$$E_i^p = g_i^p E_{i,\circ}^p + \alpha_i^q E_{i,\circ}^q \tag{7.1}$$

where $E_{i,\circ}^p$ and $E_{i,\circ}^q$ are the responses of an *ideal* antenna to the incident radiation in the p- and q-polarization states respectively. For an unpolarized source of radiation, $\langle E_{i,\circ}^p E_{j,\circ}^{q\star}\rangle = 0$. The *co-polar* visibility for such a source, measured by an interferometer using two antennas denoted by the subscripts i and j, is given by

$$\rho_{ij}^{pp} = g_i^p g_j^{p\star} \rho_{ij,\circ}^{pp} + \alpha_i^q \alpha_j^{q\star} \rho_{ij,\circ}^{qq} + \epsilon_{ij} \tag{7.2}$$

where ϵ_{ij} is independent gaussian random baseline based noise and $\rho_{ij,\circ}^{pp} = \langle E_{i,\circ}^p E_{j,\circ}^{p\star}\rangle$ and $\rho_{ij,\circ}^{qq} = \langle E_{i,\circ}^q E_{j,\circ}^{q\star}\rangle$ are the two ideal *co-polar* visibilities. ϵ_{ij} usually represents the contribution to ρ_{ij}^{pp} which cannot be separated into antenna based quantities. ϵ_{ij} therefore is a measure of the intrinsic closure errors in the system and is usually small.

[1]Strictly speaking, the ratio α_i^q/g_i^p is the correct measure of the leakage and this is what has been plotted in Fig.7.3 below. This does not however affect the computational scheme described here.

For an unpolarized point source $\langle E^p_{i,\circ} E^{p\star}_{j,\circ}\rangle = \langle E^q_{i,\circ} E^{q\star}_{j,\circ}\rangle = \rho^{pp}_{ij,\circ} = I/2$ where I is the total flux density. Writing $X^{pp}_{ij} = \rho^{pp}_{ij}/\rho^{pp}_{ij,\circ}$ we get

$$X^{pp}_{ij} = g^p_i g^{p\star}_j + \alpha^q_i \alpha^{q\star}_j + \epsilon_{ij} \tag{7.3}$$

where ϵ_{ij} now refers to the baseline based noise in X^{pp}_{ij}.

Assuming α^q_is to be negligible, the usual `antsol` algorithm estimates g^p_is such that $\sum_{\substack{i,j\\ i\neq j}} \left| X^{pp}_{ij} - g^p_i g^{p\star}_j \right|^2$ is minimized (see section 7.3). Normally, Walsh switching (Thompson et al. 1986) is used to eliminate the polarization leakage due to cross-talk between the signal paths, such that $\alpha^q_i \alpha^{q\star}_j \ll \epsilon_{ij}$. However, α^q_is can also be finite due to mechanical imperfections in the feed or the *cross-polar* primary beam, which cannot be eliminated by Walsh switching.

In the case of significant antenna based polarization leakage (compared to $\sqrt{\epsilon_{ij}}$), the second term in Equation 7.3 involving α^q_is will combine with the closure noise ϵ_{ij}. The polarization leakage therefore manifests itself as increased closure errors (see Section 7.5 for a geometric explanation on the Poincaré sphere). This has also been pointed out by Rogers (1983) in the context of VLBA observations. However, as written in Equation 7.3, the leakages and gains are actually antenna based quantities and can be solved for, using only the *co-polar* visibilities.

7.3 Algorithm and simulation

In the absence of any polarization leakage, g_is can be estimated by minimizing

$$S = \sum_{\substack{i,j\\ i\neq j}} \left| X^{pp}_{ij} - g^p_i g^{p\star}_j \right|^2 w^{pp}_{ij} \tag{7.4}$$

with respect to g_is, where $w^{pp}_{ij} = 1/\sigma^2_{ij}$, σ_{ij} being the variance on the measurement of X^{pp}_{ij}.

In Equation 7.2, if $\rho^{pp}_{ij,\circ}$ accurately represents the source structure, X^{pp}_{ij} will have no source structure dependent terms and is purely a product of two antenna dependent complex gains. For a resolved source, $\rho^{pp}_{ij,\circ}$ can be estimated from the image of the source.

Evaluating $\frac{\partial S}{\partial g^{p\star}_i}$ and equating it to zero[2] (see Appendix D), we get

[2] Complex derivatives can be evaluated by treating g^p_i and $g^{p\star}_i$ as independent variables (Palka 1990).

$$g_i^p = \frac{\sum\limits_{\substack{j \\ j\neq i}} X_{ij}^{pp} g_j^p w_{ij}^{pp}}{\sum\limits_{\substack{j \\ j\neq i}} \left|g_j^p\right|^2 w_{ij}^{pp}} \tag{7.5}$$

This can also be derived by equating the partial derivatives of S with respect to real and imaginary parts of $g_i^{p\star}$.

Since the antenna dependent complex gains also appear on the right-hand side of Equation 7.5, it has to be solved iteratively starting with some initial guess for g_js or initializing them all to 1. Equation 7.5 can be written in the iterative form as:

$$g_i^{p,n} = g_i^{p,n-1} + \lambda \left[g_i^{p,n-1} - \frac{\sum\limits_{\substack{j \\ j\neq i}} X_{ij}^{pp} g_j^{p,n-1} w_{ij}^{pp}}{\sum\limits_{\substack{j \\ j\neq i}} \left|g_j^{p,n-1}\right|^2 w_{ij}^{pp}} \right] \tag{7.6}$$

where n is the iteration number and $0 < \lambda < 1$. Convergence would be defined by the constraint $|S_n - S_{n-1}| < \beta$ (the change in S from one iteration to another) where, β is the tolerance limit and must be related to the average value of ϵ_{ij}. Equation 7.6 forms the central engine for the classical `antsol` algorithm used for primary calibration of the visibilities and in self-calibration for imaging purposes. This algorithm was suggested by Thompson & D'Addario (1982).

7.3.1 The `leaky antsol`

In the presence of significant polarization leakage, Equation 7.3 can be used to re-write Equation 7.4 as

$$S = \sum_{\substack{i,j \\ i\neq j}} \left| X_{ij}^{pp} - (g_i^p g_j^{p^\star} + \alpha_i^q \alpha_j^{q^\star}) \right|^2 w_{ij}^{pp} \tag{7.7}$$

In this form, S is an estimator for the *true* closure noise ϵ_{ij} rather than the artificially increased closure noise $(\alpha_i^q \alpha_j^{q\star} + \epsilon_{ij})$ due to the presence of polarization leakage.

Equating the partial derivatives $\frac{\partial S}{\partial g_j^{p\star}}$, $\frac{\partial S}{\partial \alpha_j^{q\star}}$ to zero, we get

$$g_i^p = \frac{\sum\limits_{\substack{j \\ j\neq i}} X_{ij}^{pp} g_j^p w_{ij}^{pp} - \alpha_i^q \sum\limits_{\substack{j \\ j\neq i}} \alpha_j^{q\star} g_j^p w_{ij}^{pp}}{\sum\limits_{\substack{j \\ j\neq i}} \left|g_j^p\right|^2 w_{ij}^{pp}} \tag{7.8}$$

$$\alpha_i^q = \frac{\sum\limits_{\substack{j \\ j\neq i}} X_{ij}^{pp} \alpha_j^q w_{ij}^{pp} - g_i^p \sum\limits_{\substack{j \\ j\neq i}} g_j^{p\star} \alpha_j^q w_{ij}^{pp}}{\sum\limits_{\substack{j \\ j\neq i}} \left|\alpha_j^q\right|^2 w_{ij}^{pp}} \tag{7.9}$$

These non-linear equations can also be iteratively solved.

Equation 7.3, which expresses the observed visibilities on a point source unpolarized calibrator in terms of the gains and leakage coefficients of the antennas, would take the same form if written in an arbitrary orthogonal basis. It is clear that the g's and the α's will change when we change the basis, so this means that the equations cannot have a unique solution. This situation is familiar from ordinary self-calibration, when only relative phases of antennas are determinate, with one antenna acting as an arbitrary reference. For observations of unpolarized sources, we can similarly say that any feed can be chosen as a reference polarization, with zero leakage, and other feeds have gains and leakages in the basis defined by this reference. Other conventions may be more convenient, as discussed in Section 7.6 which discusses degeneracy in detail.

7.3.2 Results of the simulations

We simulated visibilities with varying fraction of polarization leakage in the antennas to test the algorithm as follows. The antenna based signal and leakage were constructed as $g_i = R_g$ and $\alpha_i = f \cdot R_\alpha$ where R_g and R_α were drawn from the same gaussian random population. The visibility from two antennas i and j was then constructed as $X_{ij} = g_i g_j^\star + \alpha_i \alpha_j^\star + \epsilon_{ij}$ for $0 \leq f < 0.1$. This is equivalent to a visibility of an unpolarized point source of unit strength with a complex antenna based gain g_i and leakage α_i of strength proportional to f. Equation 7.6 was then used to compute g_i and residual χ^2 computed as $\chi^2_{\rm a} = \sum_{ij} \left|1 - \frac{X_{ij}}{g_i g_j^\star}\right|^2$. The computed values of g_i^p were then used to compute improved estimates for g_i^p by simultaneously solving for g_i^p and α_i^q using the iterative forms of Equations 7.8 and 7.9. The derived values of g_i^p and α_i^q matched the true values to within the tolerance limit. A new χ^2 was computed as $\chi^2_{\rm l} = \sum_{ij} \left|1 - \frac{X_{ij}}{(g_i g_j^\star + \alpha_i \alpha_j^\star)}\right|^2$. The values of $\chi^2_{\rm a}$ and $\chi^2_{\rm l}$ as a function of f are plotted in Fig. 7.1. The two curves become distinguishable when the leakage is significantly greater than ϵ_{ij} (for f greater than $\sim$ 1%). After that, the value of χ^2_l is consistently lower than χ^2_a, where the contribution of antenna based leakage has not been removed. Also notice that χ^2_l remains constant while χ^2_a quadratically increases as a function of f. This is due to the fact that `antsol` treats the antenna based polarization leakage as closure errors resulting in an increased χ^2 with increasing fractional leakage.

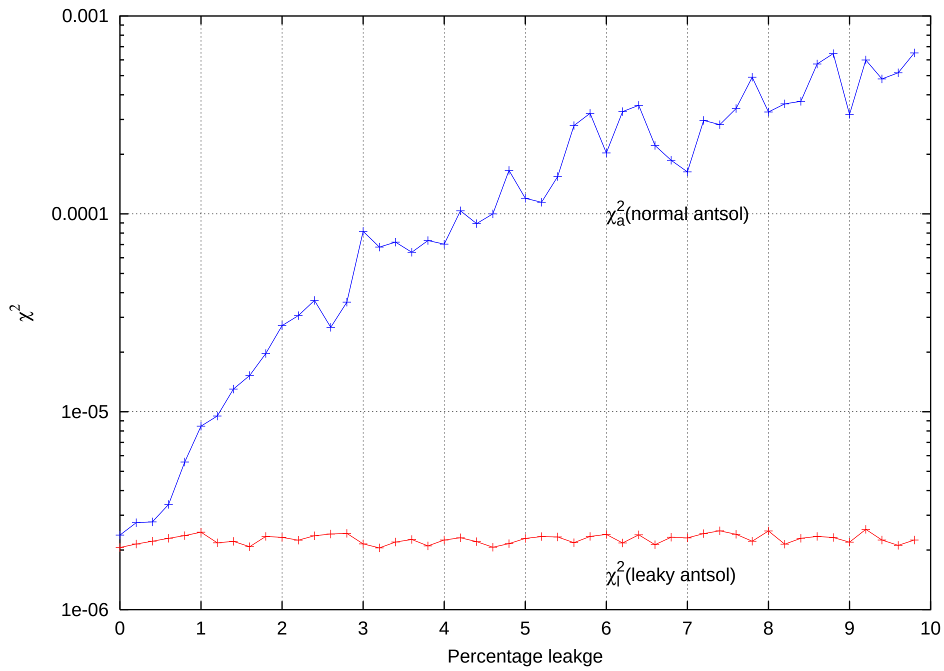

Figure 7.1: Figure showing the results of the simulations. The top curve is the value of χ^2 using the classical `antsol` (χ^2_a). The bottom curve is the value of χ^2 using the `leaky antsol` (χ^2_l) as a function of the percentage polarization leakage.

7.4 Real data

7.4.1 150 MHz data

Engineering measurements for polarization isolation at 150 MHz for the GMRT show significant polarization leakage in the system. We therefore used `leaky antsol` to calibrate the data from the Galactic plane phase calibrator `1830-36` which is known to be less than 0.2% polarized at 1.4 GHz. The percentage polarization at 150 MHz is not known, but it is expected to decrease further and it was taken to be an unpolarized point source.

Fractional polarization leakage ($|\alpha_i^q/g_i^p|$) of up to 100% was measured for most of the antennas, which is consistent with the estimated leakage measured from system engineering tests. Again, $\chi^2_{\rm a}$ and $\chi^2_{\rm l}$ were computed and the results are shown in Fig. 7.2. The 150-MHz GMRT band suffers from severe radio frequency interference (RFI). The sharp rise in the value of $\chi^2_{\rm a}$ around sample number 10 is due to one such RFI spike. This spike is present in the total power data from all antennas at this time. On an average, the χ^2 reduces by $\sim 60\%$ when leakage calibration is applied ($\chi^2_{\rm l}$). This is consistent with polarization leakage being a major source of non-closure at this frequency.

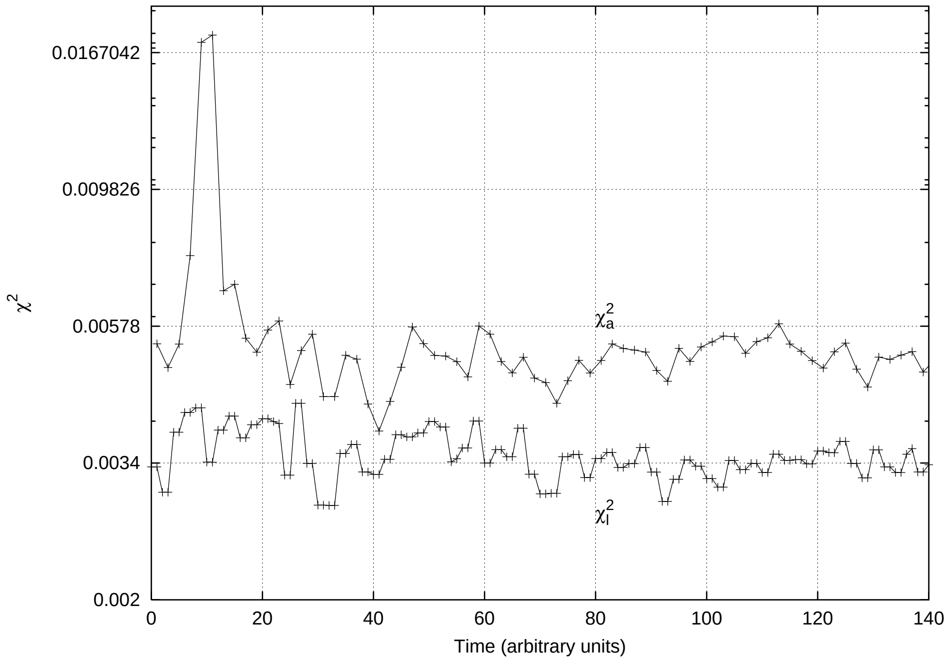

Figure 7.2: Figure showing the results using GMRT data at 150 MHz for the compact Galactic plane source `1830-36`. The top curve is the value of χ^2 using the classical `antsol` ($\chi^2_{\rm a}$). The bottom curve is the value of χ^2 using the `leaky antsol` ($\chi^2_{\rm l}$) as a function of time.

7.4.2 L-band data with circular feed

The GMRT L-band feeds are linearly polarized. For the purpose of a VLBI experiment conducted in December 2000, the L-band feed of one of the antennas was converted to a circularly polarized feed. The rest of the L-band feeds were linearly polarized and we took this opportunity to measure correlations between the circularly polarized antenna with other linearly polarized antennas using the source 3C147. Two scans of approximately one hour long observations were done using the single side band GMRT correlator. This correlator computes only *co-polar* visibilities. With this configuration of feeds, visibilities between the circularly polarized antenna and all other linearly polarized antennas corresponds to correlation between the nominal X- and R-polarizations, labeled by RX, were recorded in the first scan. The polarization of the circularly polarized antenna was then flipped for the second scan to record the correlation between the nominal X- and L-polarization states, labeled by LX.

The VLA Calibrator Manual[3] lists the percentage polarization ($\frac{\sqrt{Q^2+U^2+V^2}}{I}$) for 3C147 at L-band $< 0.1\%$. The *cross-polar* terms in Equation 7.2, which are assumed to be zero, will therefore contribute an error of the order of 0.1%. These *cross-polar* terms will be, however, multiplied by gains of type $g_i^p \alpha_i^{q\star}$. Since g_i^p and α_i^q are both assumed to be uncorrelated between antennas, this error will manifest as random noise in Equation 7.3. Within the limits of other sources of errors, the source 3C147 can therefore be considered to be a completely unpolarized source.

Results and Interpretation

The response of an ideal circularly polarized antenna to unpolarized incident radiation can be expressed as a superposition of two linear polarization states as $E^R_{i,\circ} = E^X_{i,\circ}e^{\iota\delta} + E^Y_{i,\circ}e^{-\iota\delta}$ where, the superscripts R, X and Y denote the right circular and the two linear polarization states respectively. δ is half the phase difference between the two linear polarization states and is equal to $\pi/4$ for right-circular polarization and $-\pi/4$ for left-circular polarization. Writing the general Equation 7.1 for right-circularly polarized antenna as $E^R_i = g^R_i E^R_{i,\circ} + \alpha^L_i E^L_{i,\circ}$ and substituting for $E^R_{i,\circ}$ and $E^L_{i,\circ}$ we get

$$\begin{aligned} E^R_i =& g^R_i \left(E^X_{i,\circ}e^{\iota\delta} + E^Y_{i,\circ}e^{-\iota\delta}\right) + \\ & \alpha^L_i \left(E^X_{i,\circ}e^{-\iota\delta} + E^Y_{i,\circ}e^{\iota\delta}\right) \end{aligned} \tag{7.10}$$

Equation 7.3 for the case of correlation between a circularly polarized and a linearly polarized antenna, with polarization leakage in both the antennas, can be written as

[3] The VLA Calibrator manual is available on the web from http://www.aoc.nrao.edu/~gtaylor/calib.html

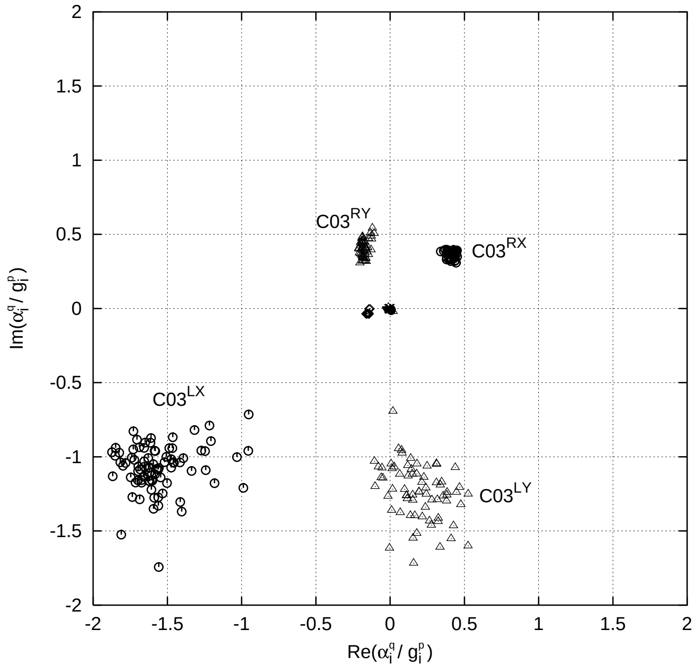

Figure 7.3: Figure showing the results using visibilities with one circularly polarized antenna and all other linearly polarized antennas at L-band. The x- and y-axis denote the real and imaginary parts of α_i^q/g_i^p respectively. g_i^p and α_i^q were solved for every integration time ($\sim 17s$). All linearly polarized antennas are close to the origin in this plot. The solutions for the circularly polarized antenna (C03) are the set of points away from the origin (shown by open circles and triangles). The two sets of points for this antenna, separated from each other by $\sim 180°$ are solutions for the right- and left-circular polarization channel. The points denoted by open circles are from correlation between the right- and left-circular polarization of C03 with nominal linear X-polarization of the other antennas (labeled as $\mathrm{C03}^{\mathrm{RX}}$ and $\mathrm{C03}^{\mathrm{LX}}$ respectively). The points denoted by triangles are from correlation of C03 with nominal Y-polarization of the other antennas (labeled as $\mathrm{C03}^{\mathrm{RY}}$ and $\mathrm{C03}^{\mathrm{LY}}$).

$$\begin{aligned} X_{ij}^{RX} =& (g_i^R e^{\iota\delta} + \alpha_i^L e^{-\iota\delta}) g_j^{X\star} + \\ & (g_i^R e^{-\iota\delta} + \alpha_i^L e^{\iota\delta}) \alpha_j^{Y\star} \\ \equiv & g_i^{X'} g_j^{X\star} + \alpha_i^{Y'} \alpha_j^{Y\star} \end{aligned} \tag{7.11}$$

where $g_i^{X'} = g_i^R e^{\iota\delta} + \alpha_i^L e^{-\iota\delta}$ and $\alpha_i^{Y'} = g_i^R e^{-\iota\delta} + \alpha_i^L e^{\iota\delta}$. The `leaky antsol` solutions for the circularly polarized antenna in this case will correspond to $g_i^{X'}$ and $\alpha_i^{Y'}$.

Let $P_i = \alpha_i^Y/g_i^X$ ($P_i = \alpha_i^{Y'}/g_i^{X'}$ for the circularly polarized antenna). Then, the amplitude of P_i is a measure of the fractional polarization leakage in the antenna while the phase of P_i gives the phase difference between the signal from one of the feeds and the leaked signal from the other feed. For an ideal circularly polarized antenna, $|P_i| \approx 1$. A plot of the real and imaginary parts of this quantity for all antennas should therefore clearly show P_i for the circularly polarized antenna with an amplitude of 1 and at an angle of $\pi/2$ with respect to the nominal X-axis.

The real and imaginary parts of P_i for all antennas from this experiment are shown in Fig. 7.3. The solutions were computed for every integration cycle of ~ 17 sec and the points on this plot represent the tip of phasor P_i. The collection of points near the origin are for all the linearly polarized antennas while the collection of two sets of points away from the origin, approximately an angle of π from each other, are for the circularly polarized antenna. The solutions found by `leaky antsol` match the expected results quite well. This therefore constitutes a reasonably controlled test with real data showing that the solutions indeed provide information about the polarization leakage in the system.

This experiment however provides much more information about the polarization properties of the antenna feeds used. The collection of points in the first quadrant denoted by open circles are the values of P_i derived from the correlation between the nominal right-circularly polarized signal and the linearly polarized signals along the nominal X-axis from all other antennas. Points in the third quadrant are similarly derived using the left-circular signals. The set of points denoted by triangles in the second and fourth quadrant are derived using correlations of right- and left-circularly polarized signals with the linearly polarized signals along the nominal Y-axis from all other antennas.

A larger spread in the solutions using the left-circularly polarized signals indicates that the closure noise (from other unknown sources) in these signals is higher. The fact that the amplitude of P_i derived using the right-circularly polarized signals is ≈ 0.5 indicates that the nominal circularly polarized feed is in fact elliptically polarized with this axial ratio. The spread of $\pm 1-2\%$ about the origin is indicative of polarization leakage at the level of few percent in the linearly polarized antennas as well. The leakage in one of the linearly polarized antennas is significantly larger ($\approx 4\%$). Since this kind of data is routinely taken on primary calibrators during GMRT observations for synthesis imaging, `leaky antsol` provides a useful diagnostic of system health, polarization performance and numbers needed to correct the data in high accuracy work.

The following test was also carried out to check that the closure phase on a triangle involving the circular feed was indeed mainly due to polarization effects. The three baselines making up this triangle were flagged as bad baselines from the input data and a new solution found for the gains and leakages of all antennas. This solution predicted the same closure phase (to within errors) as actually observed.

7.5 Closure phase and the Poincaré sphere

In this section we use right- and left-circular polarization states as the basis. A general elliptically polarized state can be written as a superposition of two states represented by the vector $\begin{pmatrix} \cos\theta/2 \\ \sin\theta/2\, e^{\iota\phi} \end{pmatrix}$. Clearly, $\theta = \pi/2$ corresponds to linear polarization and $\theta \neq 0, \pi/2$ to elliptical polarization (see Fig. 7.4). Increasing ϕ by ζ rotates the direction of the linear state or the major axis of the ellipse by $\zeta/2$. We can chose the phase of the basis so that $\phi = 0$ corresponding to linear polarization along the x-axis. The Poincaré sphere representation of the state of polarization maps the general elliptic state to the point (θ, ϕ) on the sphere. The properties of this representation are reviewed by Ramachandran & Ramaseshan (1961). We are concerned here with one remarkable property, discovered by Pancharatnam (1956, 1975). Whenever there is constructive interference between two sources of radiation, it is natural to regard them as in phase. A remarkable property of this simple definition manifests itself when we consider 3 sources of radiation of different polarization - that if a source A is in phase with B and B in phase with C, C in general need not be in phase with A. The phase difference between A and C is known in the optics literature as the geometric or Pancharatanam phase (see also Ramaseshan & Nityananda (1986); Berry (1987)). We show that this naturally occurs in radio interferometry of an unpolarized source with three antennas of different polarizations.

Let the polarization states of the three antennas be represented by $\begin{pmatrix} g_1 \\ \alpha_1 \end{pmatrix}$, $\begin{pmatrix} g_2 \\ \alpha_2 \end{pmatrix}$, and $\begin{pmatrix} g_3 \\ \alpha_3 \end{pmatrix}$ in a circular basis. Denoting the vector $\begin{pmatrix} g_i \\ \alpha_i \end{pmatrix}$ by ψ_i, one clearly see that the visibility on the 1-2 baseline is proportional to $\psi_1^\dagger \psi_2$. Hence the closure phase around a triangle made by antennas 1, 2, and 3 is the phase of the complex number (also called the triple product) $V_{123} = (\psi_1^\dagger \psi_2)(\psi_2^\dagger \psi_3)(\psi_3^\dagger \psi_1)$. In the quantum mechanical literature, this type of quantity goes by the name of Bargmann's invariant and its connection to the geometric phase was made clear by Samuel & Bhandari (1988). With some work, one can give a general proof that the closure phase (phase of V_{123}) is equal to half the solid angle

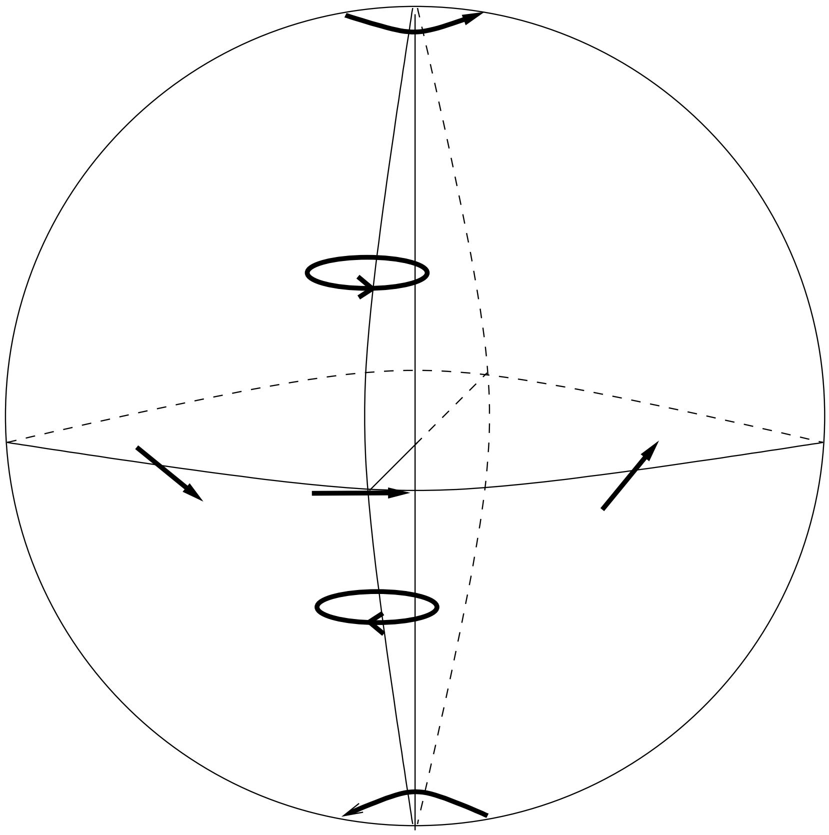

Figure 7.4: Poincaré sphere representation of the state of polarization. Poitns on north and south poles of the sphere correspond to pure right and left circular polarization. Points along the equator correspond to pure linear polarization. A linear polarization along the x-axis is represented by a point at $\theta = \pi/2$ and $\phi = 0$ while linear polarization along the y-axis is represented by a point at $\theta = \pi/2$ and $\phi = \pi/2$.

subtended at the centre of the Poincaré sphere by the points represented by ψ_1, ψ_2, and ψ_3 on the surface of the sphere. For the case where the polarization state of the three antennas are same, this phase is zero in general. However, when the polarization states of the antennas are different, this phase is non-zero.

The well known result that an arbitrary polarization state can be represented as a superposition of two orthogonal polarization states translates to representing any point on the Poincaré sphere by the superposition of two diametrically opposite states on a great circle passing through that point. For example, circular polarization can be expressed by two linear polarizations, each with intensity $1/\sqrt{2}$. In the context of the present work, the nominally circularly polarized antenna maps to a point away from the equator on the Poincaré sphere (it would be exactly on the pole if it is purely circular) while the rest of the antennas map close to the equator (they would be exactly on the equator if they are purely linear and map to a single point if they were also identical). The visibility phase due to the extra baseline based term in Equation 7.3 due to polarization mis-match is a consequence of the Pancharatanam phase mentioned above. This phase, on a triangle involving the circularly polarized antenna, will be close to the angle between the two linear antennas. For example, if $\psi_1 = \begin{pmatrix} 1 \\ \iota \end{pmatrix}$, $\psi_2 = \begin{pmatrix} 1 \\ 0 \end{pmatrix}$, and $\psi_3 = \begin{pmatrix} \cos\gamma \\ \sin\gamma \end{pmatrix}$, the phase of V_{123} will be γ. This picture can be depicted by plotting the real and imaginary parts of α_i^q/g_i^p, which is done in Fig. 7.3. The circularly polarized antenna can be clearly located in this figure as the set of point away from the origin while the linearly polarized antennas as the set of points close to the origin. The collection of points located away but almost symmetrically about the origin represents the nominal right- and left-circularly polarized feeds. Points on the equator, but significantly away from the origin represents an imperfect linearly polarized antenna. Note that the average closure phase between the nominally linear antennas is close to zero, which defines the mean reference frame in Fig. 7.3.

7.6 Non-uniqueness of solutions

We discuss the non-uniqueness of the solutions of Equation 7.3, and possible convenient conventions for choosing a specific solution. One obvious degeneracy is that multiplication of all the α's by one common phase factor independent of antenna, and all the g's, by another, in general different, common factor, does not affect the right hand side of Equation 7.3. Also, the equation was written in a specific basis, say right and left circular. But it would have had the same form when using any other orthogonal pair as basis. Hence we are free to apply this change of basis to one solution to get another solution of Equation 7.3. Under such a change, the coefficients transform according to

$$\begin{pmatrix} g' \\ \alpha' \end{pmatrix} = \begin{pmatrix} \cos\phi & e^{\iota\gamma}\sin\phi \\ -e^{-\iota\gamma}\sin\phi & \cos\phi \end{pmatrix} \begin{pmatrix} e^{\iota\zeta_1} & 0 \\ 0 & e^{\iota\zeta_2} \end{pmatrix} \begin{pmatrix} g \\ \alpha \end{pmatrix} \tag{7.12}$$

It is easy to verify that under this change, $\alpha_i'\alpha_j^{\star\prime} + g_i'g_j^{\star\prime} = \alpha_i\alpha_j^\star + g_ig_j^\star$. Clearly, since χ^2 is unchanged by these transformations, an iterative algorithm will simply pick one member of the set of possible solutions, determined by the initial conditions. Having found one such, one could apply a suitable transformation to obtain a solution satisfying some desired condition. For example, if one has nominally linear feeds, one might impose the statistical condition that there is some mean linear basis with respect to which the leakage coefficients will be as small as possible. Such a condition has the advantage that a perfect set of feeds is not described in a roundabout way as a set of leaky feeds with identical coefficients, simply because the basis chosen was different. Carrying out the minimization of $\sum |g_i|^2$ by the method of Lagrange multipliers, subject to a constant χ^2, we obtain the condition that $\sum \alpha_i^* g_i = 0$. This solution can be interpreted as requiring the leakage coefficients to be orthogonal to the gains, and is reasonable when we think about the opposite kind of situation, when the leakages are "parallel" to the gains, i.e. identical apart from a multiplicative constant. In such a case, we would obviously change the basis to make the new leakage zero. If we have a solution which does not satisfy this orthogonality condition, we can bring it about in two steps. First, choose an overall phase for the α's so that $\sum \alpha_i^\star g_i$ is real. Then, carry out a rotation in the $g - \alpha$ plane by an angle θ satisfying $\tan\theta = \sum \alpha_i^* g_i / (\sum (g_i g_i^\star - \alpha_i \alpha_i^\star)$. This rotation has been so chosen that it makes the leakage "orthogonal" to the gains, in the sense required above. Even after this is done, we still have the freedom to define the phase zero independently for the two orthogonal states. This is because we are only dealing with unpolarized sources. Of course, if we had a linearly polarized calibrator, the relative phase of right and left circular signals would not be arbitrary.

A more geometric view of this degeneracy is obtained when we think in terms of the Poincaré sphere representation of the states of polarization of all the feeds. The cross correlation between the outputs of two feeds, both of which receive unpolarized radiation, has a magnitude equal to the cosine of half the angle between the representative points on the sphere. Measurements of all such cross correlations with unpolarized radiation fixes the relative geometry of the points on the sphere, while leaving a two parameter degeneracy corresponding to overall rigid rotations of the sphere. This degeneracy can be lifted by the measurement of one polarized source at many parallactic angles.

Finally, we note that for the purpose of correcting the observations of unpolarized sources for the effects of non-identical feed polarization, the degeneracy is unimportant, because the correction factor is precisely the right hand side of Equation 7.3 which is unaffected by all the transformations we have discussed.

7.7 Conclusions

Rogers (1983) pointed out that non ideal feed polarizations of the individual antennas of a radio interferometer can result into closure errors in the *co-polar* visibilities. In this chapter we described and demonstrated a method to measure the polarization leakage of individual antennas using the nominally *co-polar* visibilities for an unpolarized calibrator. This method can therefore be used as a useful tool for studying the polarization purity of the antennas of radio interferometers from the observations of unpolarized calibrators. However, since only unpolarized calibrators are used, the actual solution for the leakage parameters is subject to a degeneracy. This degeneracy does not affect the correction of the visibilities and can be used to remove the closure errors due to polarization leakage. Massi et al. (1997) have shown that such polarization leakage induced closure errors in the data from the EVN is the dominant effect of instrumental polarization. For the EVN, this effect can be seen as a reduction in the dynamic range of the images. Our method can be used for such data to remove these closure errors for unpolarized sources.

The general elliptic state of the polarization of radiation can be represented by a point on the Poincaré sphere. The phase difference between three coherent sources of radiation but with different states of polarization goes by the name of Pancharatanam or geometric phase in the optics literature. We interpret the *co-polar* visibilities with polarization leakages on the Poincaré sphere and show that the polarization induced closure phase errors in radio interferometers is same as the Pancharatanam phase of optics. The antenna based leakages also map to points on the Poincaré sphere and the ambiguity in the solution can be understood as a rigid rotation of the Poincaré sphere, which leaves the leakage solutions unchanged relative to each other.